Zinc borate chemical garden and zinc borate powders from tincal mineral and zinc sulfate heptahydrate

Burcu Alp[1], Mehmet Gönen[2], Sevdiye Atakul Savrik[3], Devrim Balkose[4*]

[1]**Süleyman Demirel University, Department of Chemical Engineering, Isparta, 32260, Turkey,**
ORCID orcid.org/0000-0002-0380-2020
[2]**Süleyman Demirel University, Department of Chemical Engineering, Isparta, 32260, Turkey,**
ORCID orcid.org/0000-0001-5780-4622
[3]**Akzo Nobel, Izmir, 35410 Turkey, ORCID orcid.org/0000-0002-1402-0569**
[4]**Izmir Institute of Technology, Department of Chemical Engineering, Izmir, 35430, Turkey,**
ORCID orcid.org/0000-0002-1117-9486

ARTICLE INFO

ABSTRACT

The formation of the first membrane, the swelling of the crystal by incoming water from the semipermeable membrane and the formation of irregular shaped branches were observed by optical microscopy, when zinc sulfate heptahydrate crystals were immersed in saturated borax solution. The powders obtained by mixing dilute aqueous borax and zinc sulfate solutions had B, O, Na, S and Zn elements. Presence of Na $Zn_{1/2}B_4O_7 \cdot xH_2O$ was indicated by EDX analysis. The molar ratio of B_2O_3/ZnO in powders was around 2. FTIR analysis indicated the ratio of absorbance values of asymmetric stretching vibrations of $B_{(3)}$-O at 1351 cm^{-1} to that of $B_{(4)}$-O at 1026 cm^{-1} increased with their heating time at 90ºC during their preparation. X-ray diffraction patterns indicated the presence of $Zn(OH)_2$ and $Zn_4(OH)_6(SO_4) \cdot 4H_2O$. The zinc borate compounds in the powders were not crystalline since no sharp peaks related to zinc borates were present in x-ray diffraction diagram. There were two mass loss steps in TG curves of the powders. The first step at 150-350ºC and the second step at 700-950ºC were due to elimination of water and due to decomposition of sulfate ions respectively. The submicron powders were a mixture of zinc borate, $Zn(OH)_2$, $Zn_4(OH)_6(SO_4) \cdot 4H_2O$ and Na $Zn_{1/2}B_4O_7 \cdot xH_2O$ and they could be used as lubricant additive due to their small particle size of 600 nm.
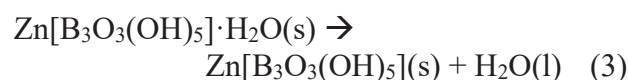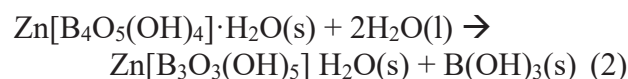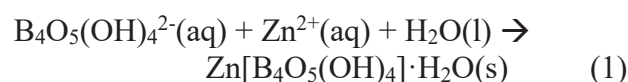
1. Introduction

Chemical gardens are the hollow fibers formed by immersion of a soluble metal-salt particle in an aqueous solution containing either of the silicate, phosphate, carbonate, oxalate, sulfide or hydroxide ions. The possible reactants in chemical gardens and their mechanism of formation are summarized by Barge et al. [1]. The gelatinous precipitate formed around the salt particle acts as a membrane and allows the passage of small water molecules and does not allow the passage of large metal ions [1]. Membrane bursts when the osmotic pressure inside becomes higher than its tensile strength. The metal-ion solution from crystal side ejects into outer solution and tubular precipitates form around the flow creating hollow chemical garden tubes [2]. Crystals of cations of group II [2] and the transition metals [3-7] were used as salts added to silicate solution. The kinetics of formation of silica garden tubes prepared using different metal salts were investigated by Glaab et al. [8]. Other solutions other than silicates

were also used in chemical gardens. Hexacyanoferrate $Fe(CN)_6^{-1}$ [9,10], OH$^-$ [11] anions are examples for this case. Real time X-ray fluorescence (XRF) movie technique was used to monitor chemical garden fiber formation [12].

Zinc borates are commercially important chemicals [13]. They can be obtained either by reaction of ZnO and H_3BO_3 [14] or reaction of borax with zinc salts [15-23].

The reactions of borate anion with zinc cation are shown below:

$$B_4O_5(OH)_4^{2-}(aq) + Zn^{2+}(aq) + H_2O(l) \rightarrow Zn[B_4O_5(OH)_4] \cdot H_2O(s) \qquad (1)$$

$$Zn[B_4O_5(OH)_4] \cdot H_2O(s) + 2H_2O(l) \rightarrow Zn[B_3O_3(OH)_5] \, H_2O(s) + B(OH)_3(s) \quad (2)$$

$$Zn[B_3O_3(OH)_5] \cdot H_2O(s) \rightarrow Zn[B_3O_3(OH)_5](s) + H_2O(l) \quad (3)$$

Kıpçak et al. [19] synthesized zinc borate using tincalconite mineral according to the following reaction in Equation 4.

$$ZnSO_4 \cdot 7H_2O + Na_2B_2O_7 \cdot 5H_2O +$$
$$3H_3BO_3 + xH_2O \rightarrow$$
$$1/3[Zn_3B_6O_{12} \cdot 3.5H_2O] +$$
$$Na_2SO_4 + 5H_3BO_3 + yH_2O \quad (4)$$
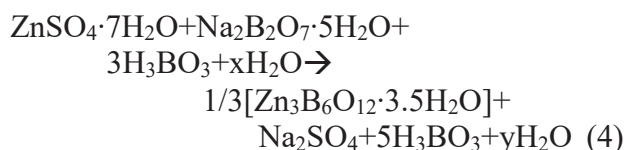
$Zn(H_2O)B_2O_4 \cdot 0.12H_2O$ was obtained from $ZnSO_4 \cdot 7H_2O$, $K_2B_4O_7 \cdot 4H_2O$, and $NH_4HB_4O_7 \cdot 3H_2O$ in H_2O with pH regulated to 9.5 with 3 mol dm^{-3} NaOH solution by Liang et al. [22].

$4ZnO \cdot B_2O_3 \cdot H_2O$ having 2D and 3D nano/microstructures were obtained by hydrothermal method in the presence of surfactant polyethylene glycol-300 from $Na_2B_4O_7 \cdot 10H_2O$ and $ZnSO_4$ [21,24]. Nano discs of $2ZnO \cdot 3B_2O_3 \cdot 3H_2O$ were obtained from aqueous borax and zinc salt solutions by the addition of oleic acid [25]. Lubricant additive zinc borate nanoparticles were obtained from borax decahydrate and zinc nitrate hexahydrate solutions by addition of sodium dodecylbenzenesulfonate [15], PEG 4000 and Span 60 [26], phosphate ester [27] as templates.

Parallel to zinc borate formation the possibility of $Zn(OH)_2$ formation according to Equation 5 was indicated by Savrik et al. [26].

$$Zn^{2+} (aq) + OH^- (aq) \rightarrow Zn(OH)_2 (s) \quad (5)$$

Polat and Sayan [28] investigated the change of properties of zinc borate with stirring rate, temperature and reactant feed rate. For zinc borate crystallization, sodium tetraborate decahydrate and zinc sulfate heptahydrate were used as reactants. The results showed that the obtained crystals were in the form of $Zn_2B_6O_{11} \cdot 7H_2O$ and the operating conditions change the size, morphology, and filtration characteristics of the zinc borate crystals. Box-Behnken design with response surface methodology showed that the data sufficiently fit the second-order polynomial model for the variables of stirring rate, temperature, and reactant feed rate. The minimum particle size (3.3 µm) was obtained at 450 rpm stirring rate, 85ºC temperature and 300 cm^3 h^{-1} reactant feed rate.

In this study, it was aimed to obtain and monitor the formation of chemical garden fibers by immersing zinc sulfate heptahydrate crystals in borax decahydrate solution prepared from purified Kırka tincal mineral. It was also aimed to characterize purified tincal mineral and to identify products in the powders formed by the reaction of dilute borax solution with dilute zinc sulfate heptahydrate solution. Elemental analysis (EDX), Fourier transform infrared spectroscopy (FTIR), X-ray diffraction (XRD), thermal gravimetric (TG) analysis and scanning electron microscopy (SEM) techniques were used for this purpose.

2. Materials and Methods

2.1. Materials

Tincal mineral from Etibank Kırka Mines, anionic flocculant SP100A (American Cynamid Company) and zinc sulfate heptahydrate (99%) from Merck were used in the experiments.

2.2. Purification of Tincal Mineral

Tincal mineral was purified from impurities by flocculation. 80 cm^3 20% tincal mineral solution was mixed with 3 cm^3 of 0.1% SP100A anionic flocculant at 80ºC. 70 cm^3 of the clear solution on top of the settled particles were transferred to another beaker and the crystals obtained by cooling were separated by filtration. They were dried at 20ºC and used in zinc borate synthesis. The flocculated particles were characterized as dolomite by Akdeniz et al. [29].

2.3. Chemical Garden Preparation and Characterization

Zinc sulfate heptahydrate crystals were immersed in saturated borax decahydrate solution at 20ºC for the formation of zinc borate chemical garden. Since it was not possible to record the photographs of the very small diameter transparent fibers by conventional photography, the same process was repeated using an optical microscope. A small crystal of zinc sulfate heptahydrate was placed on a drop of saturated borax solution at 20ºC having 4.71% borax on a microscope slide and its photographs were captured in transmission mode by a digital camera fitted to Olympus, CH40 optical microscope at different time intervals.

2.4. Preparation of Zinc Borate

50 cm^3 of 0.1 mol.dm^{-3} borax decahydrate solution was mixed with 50 cm^3 0.1 mol dm^{-3} with zinc sulfate heptahydrate at 90ºC in a thermostatic shaking water bath up to 120 minutes. Samples withdrawn at different periods were filtered and the obtained precipitates were washed with water and dried at 105ºC till constant mass was obtained.

2.5. Characterization Methods

FTIR of the samples were obtained with KBr disc method in 400-4000 cm^{-1} wavenumber range by using Shimadzu 8601 PC FTIR spectrophotometer. Setaram LABSYS TGA/DTA was used for thermal gravimetric analysis of the samples. The samples were heated from room temperature to 1000ºC at 10ºC min^{-1} rate under 40 cm^3 min^{-1} N$_2$ gas flow rate for this purpose. The powder X-ray diffraction (XRD) diagrams of the

samples were obtained by using Philips Xpert-Pro X-ray diffractometer. CuK_α radiation with 0.154 nm wavelength at 45 kV and 40 mA was used and the data was recorded in 2θ range of 2-70º. Philips XL30 SFEG scanning electron microscope was used at accelerating voltage of 5 or 6 kV to obtain the SEM micrographs of the samples coated with gold. EDX analyses of the pristine samples were made using the same instrument.

3. Results and Discussion

3.1. Characterization of Purified Borax

3.1.1. X-ray diffraction diagram of borax

X-ray diffraction diagram of borax sample used in the present study seen in Figure 1 had identical peaks with borax decahydrate (with JCPDS card number 01-75-1078) [30]. The 2θ values of the peaks were the same but their relative intensities were different than reported in the reference [30] due to orientation of the crystals. The most intense peak is at 2θ value of 34º indicated that crystals were oriented perpendicular to (024) plane [30].
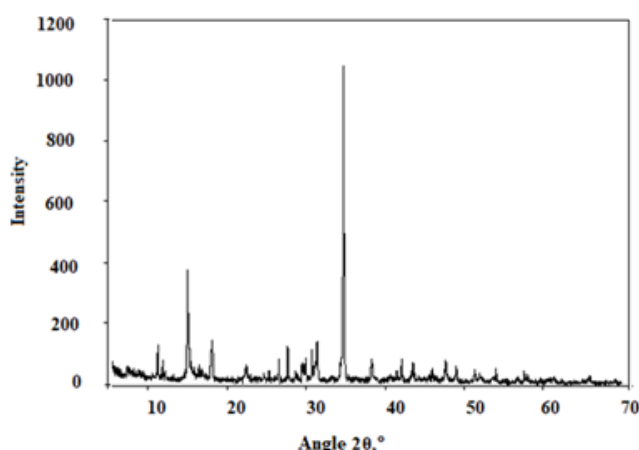

Figure 1. X-ray diffraction diagram of borax decahydrate.

3.1.2. FTIR spectrum of borax

The FTIR spectrum of borax from purified tincal mineral shown in Figure 2 confirms with the FTIR spectrum of borax decahydrate reported in literature [31,32].
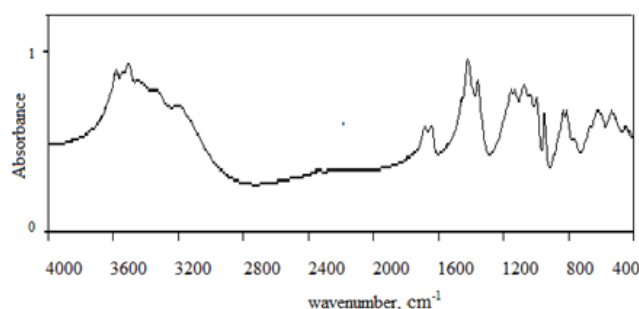

Figure 2. FTIR spectrum of borax decahydrate.

3.1.3. Morphology of borax

The SEM micrograph of borax decahydrate crystals seen in Figure 3 indicated they are in needle shape with length 5-10 μm and diameter 0.2-1 μm. The X-ray diffraction diagram also indicated one dimensional orientation of borax decahydrate crystals. This could be due to templating effect of the flocculant (Superfloc100A) used for the removal of impurities in borax mineral by flocculation.
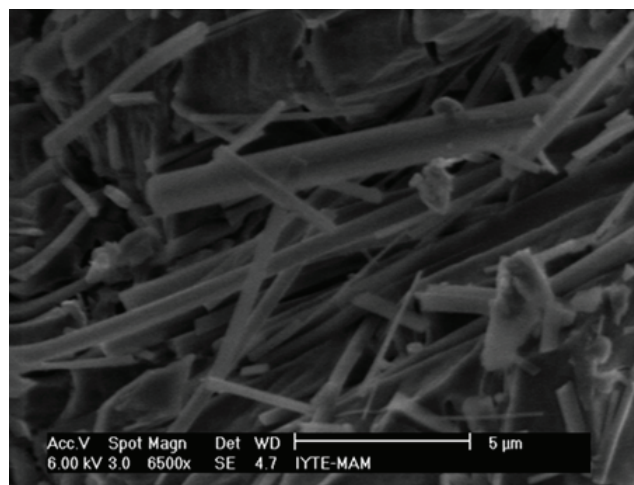

Figure 3. SEM micrograph of borax decahydrate.

3.2. Chemical Garden

Zinc sulfate heptahydrate particles were immersed in saturated borax solution at room temperature. Nearly transparent short chemical garden fibers formed in 30 minutes. Good photographs of the fibers could not be taken since they were transparent. Long fibers similar to the ones formed by immersion of zinc salts [5] and copper salts [11] to aqueous sodium silicate solution were not observed in the present case of aqueous borax zinc salt system. For this reason, it was attempted to monitor the fiber formation using an optical microscope. A small crystal of zinc sulfate heptahydrate was placed on top of a drop of saturated borax solution and the photographs were taken at different times. When zinc sulfate heptahydrate is placed in aqueous solution of borax solution it starts to dissolve to give Zn^{2+} and SO_4^{2-} ions which react with the OH^- and $B_4O_7^{2-}$ ions in solution. A semipermeable membrane made out of possible solid reaction products such as $Zn(OH)_2$, $Zn_4(OH)_6(SO_4)_2 \cdot 4H_2O$ and $2ZnO \cdot 3B_2O_3 \cdot 3H_2O$ covering the surface of sodium sulfate crystal is formed. Water can easily diffuse through the membrane creating a very high osmotic pressure in the crystal side. A saturated sodium sulfate solution forms on the surface of the crystals beneath the semipermeable membrane formed. Considering the solubility of sodium sulfate heptahydrate in water at 20ºC (3.143 mol kg^{-1}) [33] the osmotic pressure created inside of the membrane is calculated as 22.95 MPa using Equation 6.

$$\pi = icRT \qquad (6)$$

where π is osmotic pressure, i is number of ions formed by the dissociation of one mol substance, c is concentration in mol m^{-3}, R is the gas constant in J mol^{-1} K^{-1} and T is temperature in K. This high osmotic pressure first swells, then ruptures the membrane and saturated salt solution flows through the holes created on its surface into borax solution resulting formation of a new membrane with the reaction of borax and zinc sulfate. The membrane ruptures and reforms repeatedly. In crystal side of the membrane there is a concentrated zinc sulfate solution and at the other side of the membrane aqueous borax solution is present. The inside solution is ejected into outside solution at points ruptured on the membrane and thus a new membrane emanating from the center membrane is formed. Thus hollow fibers with $Zn(OH)_2$, $Zn_4(OH)_6(SO_4)_2 \cdot 4H_2O$ and $2ZnO \cdot 3B_2O_3 \cdot 3H_2O$ would form. The micrographs of the process taken from optical microscope at different time periods are shown in Figure 4. The crystal immersed in solution is covered immediately with a membrane. At zero time the size of the membrane coated crystal is 100 µm as observed in Figure 4a and 4b. The size expanded by swelling due to the inflow water through the membrane to 277 µm in 302 seconds as seen in Figure 4c. The surface of the membrane is not smooth. The growth is not the same in all directions. Two branches in 108 µm size emanated from a body of
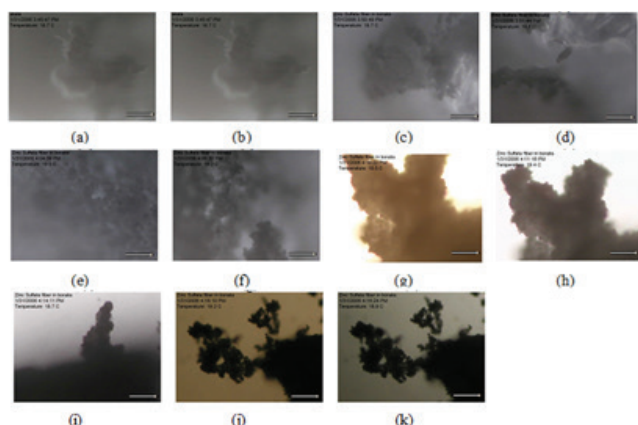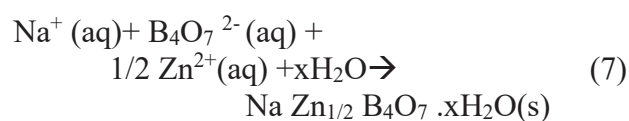

Figure 4. Optical micrographs of zinc sulfate hepta hydrate immersed in saturated borax solution at room temperature after immersion time of a and b. 0.0 , c. 302, d. 357, e. 1129, f. 1245, g.1475, h.1529, i. 1704, j.1823, k. 1837 seconds (scale bar represents 100 µm)

153 µm in 1475 s in Figure 4g. A branch with 107 µm at the bottom, 61 µm in the middle and 15 µm at the tip is seen in 1704 s in Figure 4i and particles having 31-138 µm with very tiny branches with 15 µm diameter forms in 1837 s in Figure 4k. The optical microscope had shown the formation and expansion of branches of with irregular shapes. Filtering of the fibers formed by immersing zinc sulfate heptahydrate in borax solution, washing and drying would give hallow fibers having zinc borates, $Zn(OH)_2$, $Zn_4(OH)_6(SO_4)_2 \cdot 4H_2O$.

3.3. Characterization of Powders Obtained by Mixing Aqueous Tincal Mineral and Aqueous Zinc Heptahydrate Solutions

3.3.1. Elemental analysis of the powders

EDX analysis gives information about the elemental composition of the surface of the powders. The elemental composition of the samples excluding hydrogen is shown in Table 1. In the same table molar ratios of B_2O_3/ZnO, Na/S and Na/Zn are shown. Free water molecules in the surface of the powders would be separated since the system operates under vacuum. Thus the oxygen content of the surface would be lower due to water evaporation. The samples obtained by heating for different periods at 90ºC during their preparation contained B, O, Na, S and Zn elements as shown in Table 1. The molar ratio of B_2O_3/ZnO was close to 2. The presence of S and Na elements in the samples could be due to incomplete removal of the by product sodium sulfate or due to formation of double salts. However, there was higher amount of sodium element than that is equavalent to S element to form sodium sulfate. This indicated that sodium element was present in double salts formed during the reactions. Equation 7 represents formation of a double salt by the reactants in the mixture.

$$\begin{aligned} Na^+ (aq) + B_4O_7{}^{2-} (aq) + \\ 1/2\ Zn^{2+}(aq) + xH_2O \rightarrow \\ Na\ Zn_{1/2}\ B_4O_7 \cdot xH_2O(s) \end{aligned} \qquad (7)$$

3.3.2. FTIR analysis of the powders

The FTIR spectra of the powders are shown in Figure 5. The presence of the absorption maxima at 3400 cm^{-1} for hydrogen bonded OH and at 1640 cm^{-1} for H_2O

Table 1. The elemental composition of the samples heated for different time periods at 90ºC during their preparation.

Time, minutes	B, mass (%)	O, mass (%)	Na, mass (%)	S, mass (%)	Zn, mass (%)	B_2O_3/ZnO Mol ratio	Na/S Mol ratio	Na/Zn
0	14.49	37.91	20.35	3.32	23.93	1.83	8.52	2.41
30	17.70	34.88	15.27	0.94	31.22	1.71	22.60	1.39
60	19.30	41.55	16.47	1.07	21.61	2.70	21.41	2.16
90	15.58	39.91	19.53	0.90	24.09	1.95	30.19	2.30
120	15.58	40.00	19.53	1.16	25.79	1.98	23.42	2.34

bending vibrations indicated presence of OH groups and H_2O in the samples. In the spectra of all samples the vibrations of O-B-O in planar ($B_{(3)}$-O) and vibrations of O-B-O in tetrahedral ($B_{(4)}$-O) geometries and vibrations of B-O-H are seen [19]. The ratio of absorbance of $B_{(3)}$-O vibrations at 1351 cm^{-1} to absorbance of $B_{(4)}$-O vibrations at 1026 cm^{-1} increased with heating period at 90ºC during preparation of the powder samples as shown in Table 2. This indicated the formation of planar borate ions with the expense of tetrahedral borate ions with time. Bending vibrations of B-O-H that should be observed in 1221 and 1108 cm^{-1} range overlapped with tetrahedral O-B-O vibrations. The bending vibration of planar O-B-O in ($B_{(3)}$-O) is observed at 660 cm^{-1} [19].
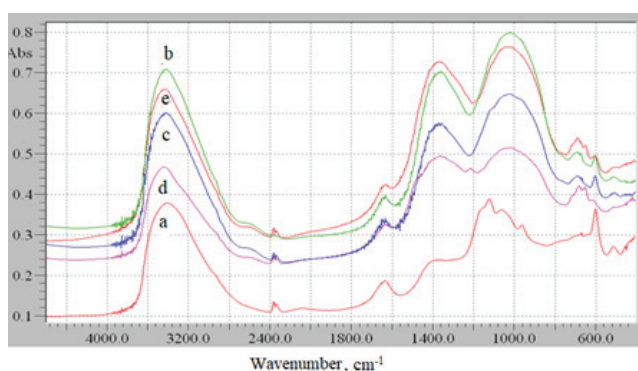
Figure 5. FTIR spectrum of the samples heated at 90ºC during preparation for heating times of a) 0, b) 30, c) 60, d) 90, e) 120 minutes.

Table 2. The ratio of absorbance of $B_{(3)}$-O asymmetric stretching vibrations at 1351 cm^{-1} to $B_{(4)}$-O asymmetric stretching vibrations at 1026 cm^{-1} for samples heated for different time periods at 90ºC during their preparation.

Time (minutes)	Intensity of 1351 cm^{-1} / Intensity of 1026 cm^{-1}
0	0.67
30	0.88
60	0.88
90	0.98
120	0.99

The presence of the bands for $Zn(OH)_2$ at 1086 cm^{-1} and 1029 cm^{-1} due to asymmetric stretching vibrations of Zn-O-Zn and at 717cm^{-1} due to bending vibrations of OH groups in $Zn(OH)_2$ indi-cated that the $Zn(OH)_2$ was also present in the powders [34]. The small sharp band observed at 600 cm^{-1} in Figure 5 could be attributed to the bending vibrations of sulfate ion that must be observed at 617 cm^{-1} [35]. The antisymmetric stretching vibrations of sulfate groups that should be observed at 1106 cm^{-1} [35] overlaps with the broad band observed for antisymmetric stretc-hing vibrations of O-B-O in $B_{(4)}$-O.

FTIR spectroscopy indicated presence of planar and tetrahedral borate groups, $Zn(OH)_2$ and sulfate groups. The FTIR spectrum of the powder formed at the first instant of mixing two reactant solutions indicated higher sulfate content than the powders obtained by further heating.
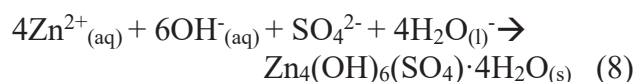
3.3.3. X-ray diffraction

X-ray diffraction diagram of the samples obtained for different heating periods are depicted in Figure 6. Sharp peaks at 2θ values of 9.4º, 18.8º, 21.6º, 25.9º, 27.4º, 29.5º, 32.9º, 34.8º, and 59.8º were observed in the X-ray diffraction diagram (curve e in Figure 6) of the sample heated for 120 minutes in its preparation. The peaks for sodium sulfate by product were also investigated since the EDX analysis indicated the presence of sulfur element. The peaks expected at 22.5º, 23.6º, 25.5º, 37.9º, 46.3º, 48.9º for sodium sulfate (JCPDS card number 36-0397) [36] were not present in Figure 6. Thus sodium sulfate was present as only in small amount as impurity. The presence of peaks at 2θ values of 31.7º, 34.3º, 36.2º (JCPDS card number 79-0206) would indicate the presence of ZnO in the samples [37]. ZnO also was not present since these peaks were absent. $Zn(OH)_2$ crystals have peaks at 2θ values of 15.4º, 15.8º, 26.0º, 27.0º, 27.8º, 29.6º, 30.9º, 31.8º, 34.2º, 36.0º, 36.3º, 37.0º, 38.4º, 39.1º, 42º, 47.1º, 48.5º and 49.3º in its XRD pattern. [34]. β-$Zn(OH)_2$ was present in the samples since most of these peaks were present in the x-ray diffraction diagram in Figure 6.
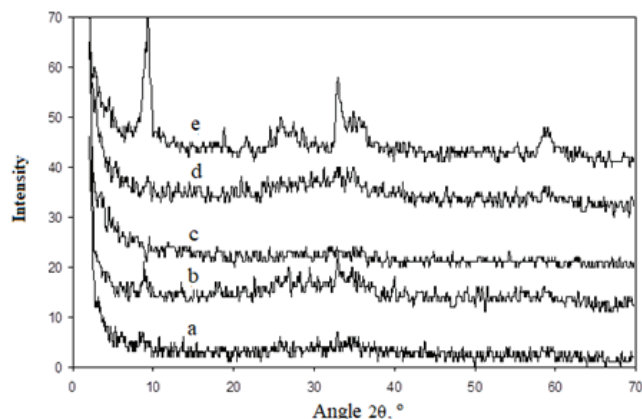
Figure 6. X-ray diffraction diagrams of the samples heated at 90ºC during preparation for heating times of a) 0, b) 30, c) 60, d) 90, e) 120 minutes.

Formation of $Zn_4(OH)_6(SO_4) \cdot 4H_2O$ [38] is another possibility in the system according to Equation 8.

$$4Zn^{2+}_{(aq)} + 6OH^-_{(aq)} + SO_4^{2-} + 4H_2O_{(l)}^- \rightarrow Zn_4(OH)_6(SO_4) \cdot 4H_2O_{(s)} \quad (8)$$

The observed X-ray diffraction peaks of the samples partially coincides with X-ray diffraction peaks of

$Zn_4(OH)_6(SO_4)\cdot4H_2O$ with ASTM Powder file 9-204 [39]. Also $2ZnO\cdot3B_2O_3\cdot3H_2O$ and $2ZnO\cdot3B_2O_3\cdot7H_2O$ peaks [40] were not present. X-ray diffraction diagrams of the samples indicated the presence of $Zn(OH)_2$ and $Zn_4(OH)_6(SO_4)\cdot4H_2O$ crystals in the samples. Even if $2ZnO\cdot3B_2O_3\cdot3H_2O$ and $2ZnO\cdot3B_2O_3\cdot7H_2O$ were present in the samples they were not in crystalline form or they had very small crystals that caused line broadening and overlapping.

3.3.4. Thermal analysis of the samples

The TG curves of the samples in Figure 7 showed two steps of mass decrease as tabulated in Table 3. The first step in 150-350ºC range is most probably due to elimination of H_2O from $Zn(OH)_2$ and $Zn_4(OH)_6(SO_4)\cdot4H_2O$ and possible zinc borate hydrates. The second step in 700-950ºC range could be due to decomposition of sulfate ions as shown below [38].

$$SO_4^{2-}\rightarrow SO_2(g)+O_2(g)+2e^- \qquad (9)$$
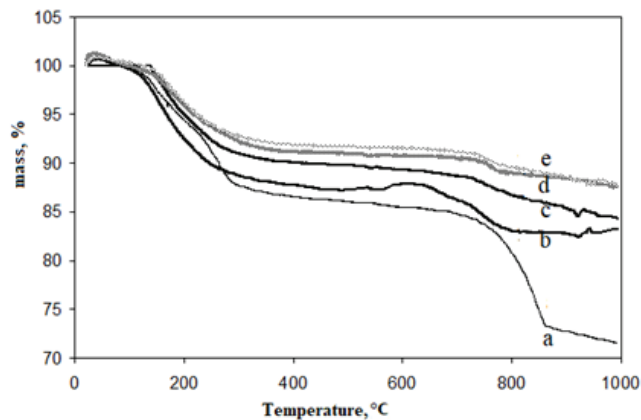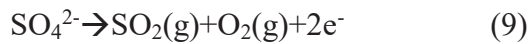
Figure 7. TG curves of crystals obtained after heating at 90ºC during preparation for heating times of a) 0, b) 30, c) 60, d) 90, e) 120 minutes.

TG analysis showed that the compounds with high water and sulfate content forms at the first instant of the reaction and the water content and sulfate content decrease as the heating period at 90ºC increases. The change in the water content of the compounds is smaller than the decrease in sulfate content with heating period. While the water content decreases from 12% to 9%, the sulfate content decreases from 10 to 1%.

3.3.5. Morphology of the samples

The SEM micrograph of the sample heated for 30 minutes at 90ºC in Figure 8 showed that it consists of agglomerated primary particles of 600 nm average diameter. The primary particles should have adhered to each other during drying process.
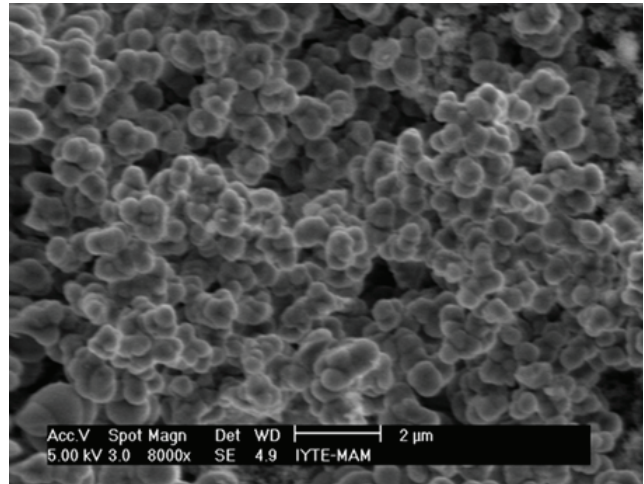
Figure 8. SEM micrograph of the sample heated for 30 minutes at 90ºC during its preparation.

3.4. Discussion

Producing zinc borates either in hallow fiber form or powder form from tincal mineral and zinc sulfate heptahydrate was investigated in this work. Since in the aqueous reaction medium OH^-, Na^+, SO_4^{2-} were also present besides $B_4O_7^{-2}$ and Zn^{2+} ions the formed powders were not pure zinc borates but they also contained $Zn(OH)_2$, $Zn_4(OH)_6(SO_4)\cdot4H_2O$ and $Na\,Zn_{1/2}\,B_4O_7\cdot xH_2O$. The x-ray diffraction diagrams showed the presence of crystalline $Zn(OH)_2$ and $Zn_4(OH)_6(SO_4)\cdot4H_2O$ phases and FTIR spectroscopy and EDX analysis indicated presence of hydrated zinc borates and $Na\,Zn_{1/2}\,B_4O_7\cdot xH_2O$. Using dilute borax decahydrate and dilute

Table 3. The temperature range and the mass % range for the step 1 and step 2 in TG curves in Figure 7 for the samples heated for different periods at 90ºC during their preparation.

Heating time minutes	Step 1			Step 2		
	Temperature range (°C)	Mass Range (%)	Mass Loss (%)	Temperature Range (°C)	Mass range (%)	Mass Loss (%)
0	150-300	100-88	12	700-850	84-74	10
30	150-260	100-91	9	650-760	88-84	4
60	150-350	100-93	7	730-940	88-85	3
90	150-350	100-92	8	730-760	91-90	1
120	150-350	100-91	9	730-760	92-91	1

zinc sulfate heptahydrate solutions (0.1 mol dm^{-3}) in the present study resulted in formation of submicron particles since there were not enough borate, zinc and OH$^-$ ions for the growth of the nucleated zinc borate, $Zn(OH)_2$ and $Zn_4(OH)_6(SO_4) \cdot 4H_2O$ particles. In studies made with higher of borax concentrations resulted well defined micron sized crystals of $Zn_3B_6O_{12} \cdot 3.5H_2O$ [24,40] or $Zn_2B_6O_{11} \cdot 7H_2O$ [27]. When boric acid was added to the mixture of aqueous sodium sulfate and borate with excess zinc ions resulted in well-defined crystals of $Zn_3B_6O_{12} \cdot 3.5H_2O$ were obtained by sonochemical method [40]. Even if the submicron particles obtained in the present study was not pure zinc borate, they can be easily dispersed in mineral oil to increase the lubrication efficiency of the mineral oil for reduction of wear of metal parts as in the study of Savrik et al [26].

4. Conclusions

The formation of chemical garden from zinc sulfate heptahydrate crystals immersed in saturated borax solution was monitored with optical microscope. The formation of the first membrane, the swelling of the crystal by incoming water from the semipermeable membrane and the formation of branches with irregular shapes were observed by optical microscopy. Thus it would be possible to obtain hallow zinc borate fibers by immersing zinc sulfate heptahydrate in saturated borax solution.

The solid reaction products obtained by mixing dilute aqueous borax and zinc sulfate solutions were attempted to be characterized in the present study. Elemental analysis indicated the presence of B, O, Na, S and Zn elements. The B_2O_3/ZnO ratio was changing around 2. Double salt formation was also possible as indicated by the high Na content of the powders. FTIR analysis showed that the ratio of absorbance of asymmetric stretching vibrations of ($B_{(3)}$-O) at 1351 cm^{-1} to absorbance of asymmetric stretching vibrations of ($B_{(4)}$-O) at 1026 cm^{-1} increased during heating of the powder during its preparation indicating tetrahedral borate ions were transformed to trihedral borate ions. Presence of $Zn(OH)_2$ and SO_4^{2-} ions in the first precipitate formed was indicated by FTIR analysis. The samples contained $Zn_4(OH)_6(SO_4) \cdot 4H_2O$ as indicated by TG analysis. X-ray diffraction confirmed the presence of $Zn(OH)_2$ and additionally presence of $Zn_4(OH)_6(SO_4) \cdot 4H_2O$. The zinc borate compounds formed were not crystalline or had very small crystals since no sharp x-ray diffraction peaks of zinc borate species were observed. The two mass loss steps at 150-350ºC and 700-950ºC ranges were due to elimination of water and the decomposition of sulfate ions respectively. The precipitate formed initially had 10% sulfate and the sulfate content decreased to 1% for the sample produced in 90 minutes heating time at 90ºC. The precipitated powder from tincal mineral and zinc heptahydrate solution was not pure. Its composition was changing with heating time during its preparation and it contained $Zn(OH)_2$, $Zn_4(OH)_6(SO_4) \cdot 4H_2O$, Na $Zn_{1/2}$ $B_4O_7 \cdot xH_2O$ besides zinc borates. The powder could be used as a lubricant additive, since it could be easily dispersed in mineral oil due to 600 nm diamemeter primary particles.

Acknowledgements

References

[1] Barge, L. M., Cardoso, S. S., Cartwright, J. H., Cooper, G. J., Cronin, L., De Wit, A., ... & Thomas, N. L. (2015). From chemical gardens to chemobrionics. *Chemical Reviews*, *115*(16), 8652-8703.

[2] Cartwright, J. H., Escribano, B., & Sainz-Díaz, C. I. (2011). Chemical-garden formation, morphology, and composition. I. Effect of the nature of the cations. *Langmuir*, *27*(7), 3286-3293.

[3] Cartwright, J. H., Escribano, B., Khokhlov, S., & Sainz-Díaz, C. I. (2011). Chemical gardens from silicates and cations of group 2: a comparative study of composition, morphology and microstructure. *Physical Chemistry Chemical Physics*, *13*(3), 1030-1036.

[4] Glaab, F., Kellermeier, M., Kunz, W., Morallon, E., & García-Ruiz, J. M. (2012). Formation and evolution of chemical gradients and potential differences across self-assembling inorganic membranes. *Angewandte Chemie*, *124*(18), 4393-4397.

[5] Balköse, D., Özkan, F., Köktürk, U., Ulutan, S., Ülkü, S., & Nişli, G. (2002). Characterization of hollow chemical garden fibers from metal salts and water glass. *Journal of Sol-Gel Science and Technology*, *23*(3), 253-263.

[6] Parmar, K., & Bhattacharjee, S. (2017). Energetically benign synthesis of lanthanum silicate through "silica garden" route and its characterization. *Materials Chemistry and Physics*, *194*, 147-152.

[7] Makki, R., Al-Humiari, M., Dutta, S., & Steinbock, O. (2009). Hollow microtubes and shells from reactant-loaded polymer beads. *Angewandte Chemie*, *121*(46), 8908-8912.

[8] Glaab, F., Rieder, J., Klein, R., Choquesillo-Lazarte, D., Melero-Garcia, E., García-Ruiz, J. M., ... & Kellermeier, M. (2017). Precipitation and crystallization kinetics in silica gardens. *ChemPhysChem*, *18*(4), 338-345.

[9] Bormashenko, E., Bormashenko, Y., Grynyov, R., Pogreb, R., & Schechter, A. (2015). How to grow a movable mini-garden in a droplet: Growing chemical gardens in a water and aqueous ethanol solutions droplets deposited on a superhydrophobic surface. *Colloids and Interface Science Communications*, *7*, 12-15.

[10] Bormashenko, E., Bormashenko, Y., Stanevsky, O.,

Pogreb, R., Whyman, G., Stein, T., & Barkay, Z. (2006). Template-assisted growth of chemical gardens: Formation of dendrite structures. *Colloids and Surfaces A: Physicochemical and Engineering Aspects*, *289*(1-3), 245-249.

[11] Escamilla-Roa, E., Cartwright, J. H., & Sainz-Díaz, C. I. (2019). Chemobrionic fabrication of hierarchical self-assembling nanostructures of copper oxide and hydroxide. *ChemSystemsChem*, *1*(3), e1900011.

[12] Zhao, W., & Sakurai, K. (2017). Realtime observation of diffusing elements in a chemical garden. *ACS Omega*, *2*(8), 4363-4369.

[13] Schubert, D. M. (2019). Hydrated zinc borates and their industrial use. *Molecules*, 24(13), 2419.

[14] Eltepe, H. E., Balköse, D., & Ülkü, S. (2007). Effect of temperature and time on zinc borate species formed from zinc oxide and boric acid in aqueous medium. *Industrial & Engineering Chemistry Research*, *46*(8), 2367-2371.

[15] Gao, P., & Zhang, Y. (2015). Synthesis and characterization of zinc borate nanowhiskers and their inflaming retarding effect in polystyrene. *Journal of Nanomaterials*, 2015.

[16] Gao, Y. H., & Liu, Z. H. (2009). Hydrothermal synthesis and standard molar enthalpy of formation of zinc borate of $4ZnO \cdot B_2O_3 \cdot H_2O$. *Journal of Chemical & Engineering Data*, *54*(9), 2789-2790.

[17] Gao, Y. H., & Liu, Z. H. (2009). Synthesis and thermochemistry of two zinc borates, $Zn_2B_6O_{11} \cdot 7H_2O$ and $Zn_3B_{10}O_{18} \cdot 14H_2O$. *Thermochimica Acta*, *484*(1-2), 27-31.

[18] Kipcak, A. S., Senberber, F. T., Derun, E. M., Tugrul, N., & Piskin, S. (2015). Characterization and thermal dehydration kinetics of zinc borates synthesized from zinc sulfate and zinc chloride. *Research on Chemical Intermediates*, *41*(11), 9129-9143.

[19] Kipcak, A. S., Senberber, F. T., Yildirim, M., Yuksel, S. A., Derun, E. M., & Tugrul, N. (2016). Characterization and physical properties of hydrated zinc borates synthesized from sodium borates. *Main Group Metal Chemistry*, *39*(1-2), 59-66.

[20] Kipcak, A. S., Acarali, N., Senberber, F. T., Yildirim, M., Koc, S. N. T., Yuksel, S. A., ... & Tugrul, N. (2016). Synthesis of dehydrated zinc borates using the solid-state method: Characterization and investigation of the physical properties. *Main Group Chemistry*, *15*(4), 301-313.

[21] Shi, X., Li, M., Yang, H., Chen, S., Yuan, L., Zhang, K., & Sun, J. (2007). PEG-300 assisted hydrothermal synthesis of $4ZnO \cdot B_2O_3 \cdot H_2O$ nanorods. *Materials Research Bulletin*, *42*(9), 1649-1656.

[22] Liang, P., Tuoheti, Z., & Liu, Z. H. (2017). Controlling the structure and morphology of zinc borate by adjusting the reaction temperature and pH value: formation mechanisms and luminescent properties. *RSC Advances*, *7*(7), 3695-3703.

[23] Nies, N. P., & Hulbert, R. W. (1970). U.S. Patent No. 3,549,316. Washington, DC: U.S. Patent and Trademark Office.

[24] Shi, X., Xiao, Y., Yuan, L., & Sun, J. (2009). Hydrothermal synthesis and characterizations of 2D and 3D $4ZnO \cdot B_2O_3 \cdot H_2O$ nano/microstructures with different morphologies. *Powder Technology*, *189*(3), 462-465.

[25] Tian, Y., Guo, Y., Jiang, M., Sheng, Y., Hari, B., Zhang, G., ... & Wang, Z. (2006). Synthesis of hydrophobic zinc borate nanodiscs for lubrication. *Materials Letters*, *60*(20), 2511-2515.

[26] Savrık, S. A., Alp, B., Üstün, F., & Balköse, D. Nano Zinc Borate as a Lubricant Additive. *Journal of the Turkish Chemical Society Section A: Chemistry*, *5*(1), 45-52.

[27] Zheng, Y., Tian, Y., Ma, H., Qu, Y., Wang, Z., An, D., ... & Gao, X. (2009). Synthesis and performance study of zinc borate nanowhiskers. *Colloids and Surfaces A: Physicochemical and Engineering Aspects*, *339*(1-3), 178-184.

[28] Polat, S., & Sayan, P. Box–Behnken experimental design for zinc borate $Zn_2B_6O_{11} \cdot 7H_2O$. *Journal of Boron*, *5*(3), 152-161.

[29] Akdeniz, Y., Özmihci, F., Duvarcı, O. Ç., Balköse, D., Ülkü, S. (2003, September 3-6). *Kırka tinkal mineralinin sulu çözeltilerindeki kolloidal fazın karakterizasyonu [Characterization of colloidal phase of Kırka tinkal mineral solution in water]*. In 11th Symposium of Clay, İzmir, Turkey.

[30] Goel, N., Sinha, N., & Kumar, B. (2013). Growth and properties of sodium tetraborate decahydrate single crystals. *Materials Research Bulletin*, *48*(4), 1632-1636.

[31] Jun, L., Shuping, X., & Shiyang, G. (1995). FT-IR and Raman spectroscopic study of hydrated borates. *Spectrochimica Acta Part A: Molecular and Biomolecular Spectroscopy*, *51*(4), 519-532.

[32] Polat, S., & Sayan, P. Effects of polyelectrolytes on the hardness of borax decahydrate crystals. *Journal of Boron*, *4*(4), 172-179.

[33] Steiger, M., & Asmussen, S. (2008). Crystallization of sodium sulfate phases in porous materials: the phase diagram $Na_2SO_4–H_2O$ and the generation of stress. *Geochimica et Cosmochimica Acta*, *72*(17), 4291-4306.

[34] Top, A., & Çetinkaya, H. (2015). Zinc oxide and zinc hydroxide formation via aqueous precipitation: Effect of the preparation route and lysozyme addition. *Materials Chemistry and Physics*, *167*, 77-87.

[35] Zhou, J., Santambrogio, G., Brümmer, M., Moore, D. T., Wöste, L., Meijer, G., ... & Asmis, K. R. (2006). Infrared spectroscopy of hydrated sulfate dianions. *Journal of Chemical Physics*, *125*(11), 111102-111102.

[36] Linnow, K., Zeunert, A., & Steiger, M. (2006). Investigation of sodium sulfate phase transitions in a porous material using humidity-and temperature-controlled X-ray diffraction. *Analytical Chemistry*, *78*(13), 4683-4689.

[37] Egbuchunam, T., & Balkose, D. (2012). Effect of super-critical ethanol drying on the properties of zinc oxide nanoparticles. *Drying Technology*, *30*(7), 739-749.

[38] Staminirova, T., Petrova, N., & Kirov, G. (2016). Thermal decomposition of zinc hydroxy-sulfate-hydrate minerals. *Journal of Thermal Analysis and Calorimetry*, *125*(1), 85-96.

[39] Bevins, R. E., Turgoose, S., & Williams, P. A. (1982). Namuwite, (Zn,Cu)4SO4(OH)6·4H2O, a new mineral from Wales. *Mineralogical Magazine*, *46*(338), 51-54.

[40] Ersan, A. C., Kipcak, A. S., Ozen, M. Y., & Tugrul, N. (2020). An accelerated and effective synthesis of zinc borate from zinc sulfate using sonochemistry. *Main Group Metal Chemistry*, *43*(1), 7-14.